Physica D 238 (2009) 253–263

Contents lists available at ScienceDirect

Physica D

journal homepage: www.elsevier.com/locate/physd

Multistability of clustered states in a globally inhibitory network

Lakshmi Chandrasekaran, Victor Matveev, Amitabha Bose *

Department of Mathematical Sciences, New Jersey Institute of Technology, Newark, NJ 07102, United States

ARTICLE INFO

Article history:
Received 3 July 2008
Received in revised form
15 October 2008
Accepted 16 October 2008
Available online 29 October 2008
Communicated by S. Coombes

Keywords:
Neuronal network
Synaptic depression
Periodic orbit
Dynamical systems

ABSTRACT

We study a network of m identical excitatory cells projecting excitatory synaptic connections onto a single inhibitory interneuron, which is reciprocally coupled to all excitatory cells through inhibitory synapses possessing short-term synaptic depression. We find that such a network with global inhibition possesses multiple stable activity patterns with distinct periods, characterized by the clustering of the excitatory cells into synchronized sub-populations. We prove the existence and stability of n-cluster solutions in a m-cell network. Using methods of geometric singular perturbation theory, we show that any n-cluster solution must satisfy a set of consistency conditions that can be geometrically derived. We then characterize the basin of attraction of each solution. Although frequency dependent depression is not necessary for multistability, we discuss how it plays a key role in determining network behavior. We find a functional relationship between the level of synaptic depression, the number of clusters and the interspike interval between neurons. This relationship is much less pronounced in the absence of depression. Implications for temporal coding and memory storage are discussed.

1. Introduction

Considerable attention has been given to the idea that neurons convey information in their patterns of activity to downstream targets. There are two general ways in which this information is transmitted. One way is through the firing rate of individual or groups of neurons. In this scenario, downstream neurons interpret the changes in firing rate to discern the behavior of the upstream network. Place cells in the hippocampus of rats are one example of cells that increase their firing rate when the animal is in a certain place or location of a known environment [18]. The second way that neurons may transmit information is through their spike times [2]. For example, two neurons may fire at the same rate, but a downstream target neuron may determine the degree of synchrony of the cells based on the difference of their spike times. Coincidence detection is a classic example of this phenomena whereby a downstream target neuron will only fire if it receives inputs from different neurons within a very small window of time.

The ability of a network of neurons to be able to convey multiple pieces of information (temporal codes) is of paramount importance given that the brain is of finite size. For reasons of efficiency it is advantageous for a single network to be able to create, store and transmit multiple codes rather than just one. This leads to the question of how these codes are constructed within the neuronal network and how does a network decide which code to transmit. Mathematically, it is equivalent to asking a very straightforward and general question: What are the circumstances under which a neuronal network exhibits multistability of solutions, i.e. several distinct stable activity states?

In this paper, we consider a globally inhibitory network of spiking neurons that is loosely based on the CA1 hippocampal structure. The network consists of m uncoupled pyramidal cells that each has an excitatory synapse onto a common interneuron. The interneuron sends inhibition that exhibits short-term synaptic depression (STSD) to each of the pyramidal cells. STSD is a transient activity-dependent decrease in synaptic strength observed in a wide variety of neural systems, characterized by frequency dependence of its effect [1]. Namely, if a pre-synaptic neuron fires at a high-frequency, then the efficacy or strength of its synapse onto post-synaptic neurons is weakened (depressed). Alternatively, if the pre-synaptic cell fires at a lower frequency, or if there is a long interspike interval, then the synapse has a longer time to recover from depression between the spikes, leading to larger synaptic efficacy, and the synapse is said to be strong. The globally inhibitory network considered here is an extension of the $E - I$ model consider in Bose et al. [3]. There we showed how STSD allows bistability between a low-frequency and a hi-frequency periodic solution. STSD allowed the frequency of these two solutions to be dependent on two sets of independent parameters; one set is associated with the inhibitory synapse and the other set is associated with the E cell.

In this paper, we show that a globally inhibitory network can exhibit multiple stable solutions, all for the same set of parameters. In particular, we show that in a network of m pyramidal cells, there

* Corresponding author.
E-mail addresses: lc42@njit.edu (L. Chandrasekaran), matveev@njit.edu (V. Matveev), bose@njit.edu (A. Bose).

0167-2789/$ – see front matter © 2008 Elsevier B.V. All rights reserved.
doi:10.1016/j.physd.2008.10.008

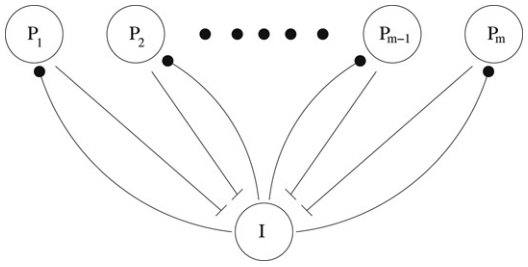

Fig. 1. An m-cell globally inhibitory network. Each synapse from P to I is excitatory, and each synapse from I to P is inhibitory and displays short-term synaptic depression.

can exist stable cluster solutions of size $n \leq m$ for any n. A n-cluster solution is one in which the network breaks up into n out-of-phase groups. Within each group the cells are fully synchronized, but the clusters are separated by a well defined interspike (intercluster) interval. Although the multistability of solutions does not explicitly depend on STSD, synaptic depression plays an important role in the properties of the ensuing solutions. In particular, STSD increases the difference between the interspike intervals and the corresponding periods of distinct clustered solutions. We will show that the equilibrium interspike interval is fully determined by the extent of synaptic depression associated with each solution, and in general decreases with the number of clusters. Thus, STSD allows there to be m different interspike intervals corresponding to m different clustered solutions, implying that the network can transmit m different codes. We will show that in the absence of depression, the separation of interspike intervals is not necessarily guaranteed. STSD also allows the network to display a further bistability of distinct solutions having the same number of clusters, qualitatively similar to that described in [3]. This work adds to that of Rubin and Terman [21] who study a globally inhibitory network of bursting cells.

The paper is organized as follows: In Section 2, we describe the mathematical model that we use for cells, as well as the model for synaptic depression. We also exploit time-scale separations to reduce the analysis to a particular slow manifold of the system. In Section 3, we first show a few simulations of clustering, and then follow up with mathematical analysis proving the existence and stability of n-cluster solutions. The basin of attraction of these solutions is analyzed, and a one-dimensional map-based approach for finding solutions is presented. We then compare our results to the situation where there is no depression in the inhibition from the global inhibitor. Throughout this section, we use a combination of analysis, simulations and numerical solutions of derived equations. The paper concludes with a brief discussion.

2. Model

We consider uncoupled pyramidal cells which make excitatory synapses onto a common interneuron; Fig. 1. We note that this architecture is effectively equivalent to an all-to-all mutually coupled inhibitory network. The interneuron sends a depressing synapse onto each of the pyramidal cells. The general set of equations that governs the activity of each pyramidal cell and the interneuron are given by

$$\begin{aligned} \epsilon \frac{dv}{dt} &= f(v, w) \\ \frac{dw}{dt} &= \frac{w_\infty(v) - w}{\tau_w(v)} \end{aligned} \tag{1}$$

where $\epsilon \ll 1$. v is the membrane potential of the cell and f is the nonlinear term which contains various ionic currents. The term $w_\infty(v) - w$ is associated with the opening and closing of potassium channels within the cell. The term $\tau_w(v)$ is the voltage-dependent w decay time constant.

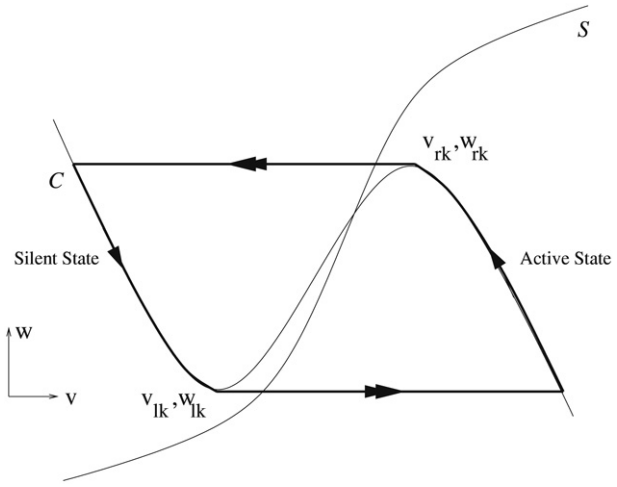

Fig. 2. Pyramidal cell $v-w$ phase plane and singular orbit. The double arrows denote a fast transition between silent and active states. A single arrow denotes the slower transition in each of those states.

The nullclines of the above Eq. (1) are obtained by setting the right hand side equal to zero. The v nullcline is a cubic-shaped curve denoted by C as shown in Fig. 2. The local max and min values are denoted (v_{rk}, w_{rk}) and (v_{lk}, w_{lk}), respectively, where the subscripts "*rk*" and "*lk*" denote the right- and the left knee of the C nullcline, respectively. The right (left) branch of C corresponds to the active (silent) state of the neuron. The w nullcline is an increasing sigmoid denoted by S.

We assume the following: Above and below the curve C, $f < 0$ and $f > 0$, respectively. Below (above) S, $(w_\infty - w) > 0$ (< 0). Near the left branch of the v nullcline where $f = 0$ we require $\frac{\partial f}{\partial w} < 0$ and $\frac{\partial f}{\partial v}$ to be nonzero everywhere except at the minimum of the nullcline. This minimum is defined by the conditions $f = 0$ and $\frac{\partial f}{\partial v} = 0$. If S intersects C at only one point and this intersection takes place in the middle branch of C then it is an unstable fixed point causing the cell to undergo oscillations. We will choose parameters such that an isolated P cell has nullclines with this geometry; Fig. 2. If S intersects C on either the left or the right branch, then the fixed point is stable. We choose parameters so that the interneuron I has a fixed point on its left branch.

Eq. (1) possesses a stable periodic solution if its fixed point lies on the middle branch. By taking ϵ to be small it is easy to construct this solution using geometric singular perturbation theory. Let $\epsilon \to 0$ in Eq. (1) to obtain the slow subsystem:

$$\begin{aligned} 0 &= f(v, w) \\ \frac{dw}{dt} &= \frac{w_\infty(v) - w}{\tau_w(v)}. \end{aligned} \tag{2}$$

Now if time is rescaled to $t = \epsilon\tau$ and then if $\epsilon \to 0$, we obtain

$$\begin{aligned} \frac{dv}{d\tau} &= f(v, w) \\ \frac{dw}{d\tau} &= 0. \end{aligned} \tag{3}$$

The singular periodic orbit consists of 4 parts. There are two slow (solutions of (2)) and two fast (solutions of (3)) parts. These fast transitions are initiated from the right and left knees of the v nullcline; Fig. 2. If ϵ is sufficiently small in the original Eq. (1) then we obtain a relaxation oscillation. In this case, the periodic orbit lies $O(\epsilon)$ close to the singular solution [16].

Before describing the coupled equations, we make an assumption to force our P cells to display spiking behavior. As in [11], we

take $\tau_w(v)$ to be small whenever $v > v_{rk}$. This will cause each P cell to spend a small amount of time in the active state and thus will reduce the width of its action potential.

2.1. Coupled equations

Each pyramidal cell receives inhibitory input from the interneuron whenever the latter fires. The interneuron, in turn, receives excitatory input whenever a pyramidal cell fires. We will assume that the I cell fires if and only if a P cell fires. Each P cell obeys

$$\begin{aligned}\epsilon\frac{dv_p}{dt} &= f(v_p, w_p) - \bar{g}_{inh}s(t-\Delta t)[v_p - E_{inh}]\\ \frac{dw_p}{dt} &= \frac{w_\infty(v_p) - w}{\tau_w(v_p)},\end{aligned} \tag{4}$$

while the interneuron obeys

$$\begin{aligned}\epsilon\frac{dv_I}{dt} &= f(v_I, w_I) - \bar{g}_{exc}s_\infty(v_p)[v_I - E_{exc}]\\ \frac{dw_I}{dt} &= \frac{w_\infty(v_I) - w}{\tau_w(v_I)}.\end{aligned} \tag{5}$$

The parameters $\bar{g}_{inh}$, $\bar{g}_{exc}$, E_{inh} and E_{exc} denote maximum synaptic conductances and the reversal potentials of the relevant synapses. Note that E_{inh} is below the resting potential, while E_{exc} is above the resting potential of the cell (see Appendix for parameter values). In our model, the excitatory synapse from any P to I is non-depressing. For simplicity, we assume that each is instantaneous and thereby model it using s_∞ given by

$$s_\infty(v_p) = \begin{cases}0, & v_p \le v_\theta\\ 1, & v_p \ge v_\theta,\end{cases} \tag{6}$$

where v_θ is a synaptic threshold lying between v_{lk} and v_{rk}.

The inhibitory synapse from I to any P is modeled as a depressing synapse. This means that the effective maximum strength of the synapse is a function of the frequency of the interneuron. Whenever I fires, the synapse depresses or weakens. Between spikes of I the synapse recovers. Thus if I fires with high frequency, then its synapse is weak. If it fires at low frequency, then its synapse will be strong. To model this, for our analysis, we use a standard phenomenological model due to Abbott et al. [1]. We use a variable D to measure the extent of depression of the synapse and another variable s to incorporate the effect of the synapse onto the P cells. Both depend on the activity of I. In between spikes of I, D recovers toward the value one with time constant τ_D.

$$\frac{dD}{dt} = \frac{1-D}{\tau_D}. \tag{7}$$

When I spikes at say $t = \hat{t}$, we reset D to rD, where $0 < r < 1$. Specifically, $D(\hat{t}^+) = rD(\hat{t}^-)$. At an I spike, the synaptic variable s is set to D by $s(\hat{t}^+) = D(\hat{t}^-)$. Between spikes of I, s decays toward zero with time constant τ_s.

$$\frac{ds}{dt} = \frac{-s}{\tau_s}. \tag{8}$$

Note that in (4), the variable s appears with a delay of Δt, $s(t-\Delta t)$. Delay of the inhibitory synapse is a necessary condition to obtain stable synchrony for fast rising synapses [25] and will play an important role in the stability of the clustered solutions obtained here.

The Abbott model for D and s assumes that each action potential has zero spike width. However, the simulations in this paper utilize a biophysical model of a CA1 pyramidal cell due to Ermentrout and Kopell [7] that have a non-zero spike width. In the Appendix we show the equations that are used for simulations and discuss what modifications on the variables D and s are necessary to incorporate non-zero spike width.

2.2. Reduction to slow manifold

We make three main assumptions to conduct the analysis

(A1) I fires if and only if any P cell fires.
(A2) Spikes of either P or I have zero time width.
(A3) Inhibition affects each pyramidal cell only when the cell is in its silent state.

It should be noted that assumptions A2 and A3 are just for ease of the analysis. Relaxing either or both of them does not qualitatively change the results. The practical effect of A3 is that when a P cell returns to the silent state, it does so with $w = w_{rk}$, the value of the local maximum of the cubic-shaped v nullcline C (Fig. 2). Assumption (A1), while not necessary to obtain clustering, drastically simplifies the analysis allowing us to focus only on the spike times of the P cells. Specifically, we can ignore the I dynamics altogether and simply track how its synapses onto each P affect the network behavior.

Due to these assumptions, we can understand the dynamics of the entire system by focusing on the behavior of the P cells in their silent state. To do that, we define a two-dimensional w–g slow manifold on which we study the evolution of the P cells. Define $g(t) = \bar{g}_{inh}s(t-\Delta t)$, where g denotes the conductance of the inhibitory synapse. To simplify the analysis, we further assume that near the left branches of the v-nullcline, $w_\infty(v) = 0$. As a result of these assumptions, the pyramidal cell P obeys a specific set of slow equations when it is in its silent state and in between spikes of I.

$$\begin{aligned}0 &= f(v, w) - g[v - E_{inh}]\\ w' &= -\frac{w}{\tau_w}\\ g' &= -\frac{g}{\tau_s}\\ D' &= \frac{1-D}{\tau_D}.\end{aligned} \tag{9}$$

Since $\frac{\partial f}{\partial v} - g$ is nonzero for all points except at the knees of the nullcline, the first equation of (9) can be solved for v in terms of w and g along the entire left branch of the nullcline, $v = F(w, g)$. This equation is valid for P in the silent state. The second and third equations of (9) are used to find the evolution of w and g which can then be used to calculate v. Note that increasing the value of the inhibitory synaptic conductance g lowers the v nullcline in the v-w phase plane.

The two dimensional w–g slow manifold (Fig. 3) has five boundaries: (1) the line $g = 0$ which occurs when a P cell receives no inhibition; (2) the line $g = \bar{g}_{inh}$, this is the value of maximum inhibition that a P cell can receive; (3) the fixed point curve which represents the points of intersection of the w nullcline with the left branches of the v nullclines corresponding to different values of g. This curve of critical points exists only for particular interval of $g \in [\hat{g}, \bar{g}_{inh}]$ where the value $\hat{g}$ is the minimum value of g for which the v nullcline intersects the w nullcline; the cell's w value is not changing along this curve; (4) the jump curve that represents the w position of the local minimum of the v nullcline corresponding to different values of g; upon reaching this curve, a cell jumps from the silent left branch to the active right branch of the v-nullcline. The slope of the jump curve is negative as is shown in [25]; (5) the return curve $w = w_{rk}$ where each P cell returns to from its active state. The return curve is vertical, by assumption (A3) as inhibition affects only the left branch of the cubic-shaped nullcline C and not the right branch.

In Fig. 3, we show an example of representative trajectories from two P cells on the slow manifold. At any moment in time, both cells receive the same amount of inhibition and thus lie on the same horizontal g-level line. Assume for a moment that the

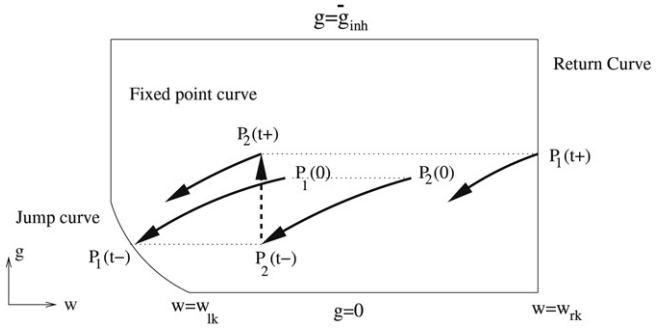

Fig. 3. Representative trajectories on the w–g slow manifold. Two cells begin at $t = 0$ and evolve toward the jump curve. When P_1 hits the curve at $t = t^-$, it is reset to $w = w_{rk}$ at $t = t^+$, while P_2 is reset vertically to the position shown. The cells then continue to evolve toward the jump curve. The dotted horizontal lines show that at any moment in time, the cells lie on the same g-level.

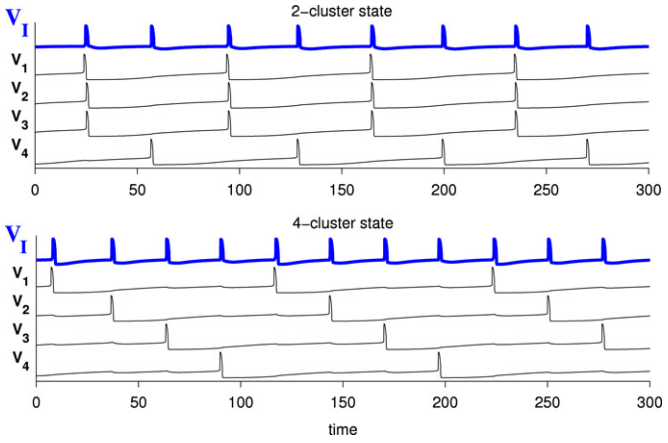

Fig. 4. Clustered solutions in a 4-cell network. In each set, the top trace V_I is for the interneuron and the remaining four are for the pyramidal cells.

synaptic delay from I to P is $\Delta t = 0$. If the cells start as shown at $t = 0$ and P_1 reaches the jump curve at $t = t^-$, then at t^+, both P_1 and P_2 are reset to $g(t^+) = \bar{g}D(t^-)$ (because I fires whenever any P fires). P_2 is reset vertically, so its w value is unchanged, while P_1 is reset to the return curve $w = w_{rk}$ representing that it has spiked.

We will be interested in the steady state behavior of the network. It turns out that clustered solutions are periodic solutions of the governing equations. This means that I fires periodically with a determinable interspike interval. As we will show below, the length of the interspike interval will depend on the number of clusters as well as various network parameters. We can calculate the maximum and minimum values that the depression and synaptic variables take over one cycle of a periodic solution. The minimum D value occurs just after an I spike, while the maximum occurs just prior to an I spike. Denote the interspike interval of I by t_{in}. Suppose at $t = 0$ a spike has just occurred and $D(0^+) = D_{\min}$. On the interval $t \in (0, t_{in})$, D follows (9), so $D(t_{in}^-) = 1 - (1 - D_{\min})\exp(-t_{in}/\tau_D)$. After the next I spike, $D(t_{in}^+) = rD(t_{in}^-)$. Thus by periodicity, we require $D_{\min} = rD(t_{in}^-)$. Solving for $D_{\min}$ yields

$$D_{\min} = \frac{r(1 - \mathrm{e}^{-t_{in}/\tau_D})}{1 - r\mathrm{e}^{-t_{in}/\tau_D}}, \tag{10}$$

from which it easily follows that $D_{\max}$ obeys

$$D_{\max} = \frac{1 - \mathrm{e}^{-t_{in}/\tau_D}}{1 - r\mathrm{e}^{-t_{in}/\tau_D}}. \tag{11}$$

It should be noted that in both equations above, the period t_{in} is not *a priori* known. In fact, in the analysis below we will determine t_{in} and show that it depends on the cluster size.

If we denote the right-hand side of (11) by $h(t_{in})$, it is easy to check that $\mathrm{d}h/\mathrm{d}t_{in} > 0$. Therefore $D_{\max}$ increases with t_{in} and $h(t_{in})$ can be inverted to solve for t_{in} as a function of $D_{\max}$.

3. Results

In Fig. 4, we show two sets of voltage traces from a 4-cell network. The bottom trace shows a stable 4-cluster solution. Notice that the distance between successive spikes is small. The interspike interval in this case is about 27 ms. The top trace shows a stable 2-cluster solution in the 4-cell network with interspike interval of 34 ms. In this simulation, three cells have synchronized, but remain out of phase with the other cell. The cluster sizes and the specifics of why a particular cell is within a particular cluster has to do with our choice of initial conditions. By changing initial conditions, we could, for example, obtain a 2-cluster solution with each cluster containing two cells. Note that the distance between spikes is larger in the 2-cluster case, as can be seen by viewing the activity of I given by the v_I trace. Both simulations are obtained for the same set of parameters (see Appendix). Moreover, in simulations not shown we can obtain 1- and 3-cluster solutions as well, with corresponding interspike intervals of 70 and 30 ms. The distance between spikes decreases with the number of clusters in the network. Further, the size of an individual cluster does not affect this distance, since I fires exactly once upon the firing of all cells in each cluster, independent of how many cells are in a cluster. Below, we will mathematically explain why this network is capable of producing multistability of solutions.

3.1. Existence of a n-cluster solution

We first prove the existence of a 2-cluster solution. For this argument we need only consider two P cells. We shall also assume that the synaptic delay from I to P is $\Delta t = 0$, a condition we will later relax when discussing stability of solutions. To prove the existence of the 2-cluster solution, we will derive two different necessary conditions and show that when both are satisfied, the solution exists.

Assume that at $t = 0$, the leading cell starts on the w–g slow manifold at (w_0, g_0), while the trailing cell starts at (w_{rk}, g_0). There exists a time $t_{g_0}(w_0)$ for the leading cell to reach the jump curve. We would like to determine if the trailing cell can reach the original w location of the leading cell, w_0, after this time. That is we want to determine if there exists a w_0 such that

$$w_{rk}\mathrm{e}^{-t_{g_0}(w_0)/\tau_w} = w_0. \tag{12}$$

If we fix g_0 and let the initial position of the leading cell approach the jump curve, $t_{g_0}(w_0) \to 0$. In this limit, the trailing cell starting at w_{rk} would need a large amount of time to reach w_0. Alternatively, if we let the initial position of the leading cell approach the return curve, then in this limit, $t_{g_0}(w_{rk}) > t_0(w_{rk})$ where the latter time satisfies $w_{lk} = w_{rk}\exp(-t_0(w_{rk})/\tau_w)$. Now the trailing cell would need very little time to reach the initial position w_0. Moreover, as w_0 is smoothly increased from the jump curve to w_{rk}, the time $t_{g_0}(w_0)$ is a strictly increasing function. Thus by the intermediate value theorem and monotonicity, there exists a unique value $w_0 = w^\star$ such that $t_{g_0}(w^\star)$ satisfies (12).

The above argument holds for any initial value of g_0. Thus we can extend it to any $g \in [0, \bar{g}]$. Doing so allows us to establish the existence of a curve $\mathcal{C}_w = \{(w, g) : w = w^\star(g_0)\}$ for which the time for the leading cell from this curve to reach the jump curve is exactly the time for the trailing cell to reach $w^\star$ satisfying (12); Fig. 5. Thus if one cell starts on $\mathcal{C}_w$ and the other at w_{rk}, both with the same g_0 value, then in the time $t_{g_0}(w^\star)$ the leading cell reaches

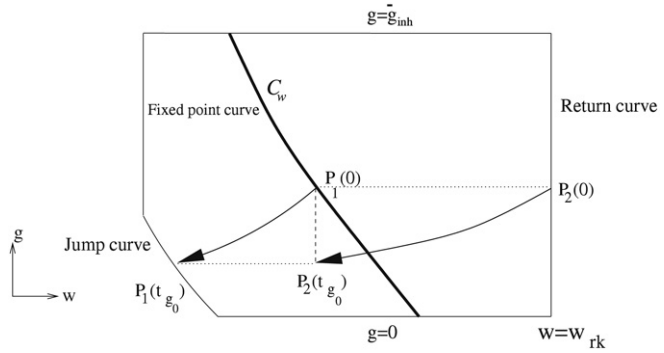

Fig. 5. The curve $\mathcal{C}_w$ on the w–g slow manifold. If the leading cell begins on $\mathcal{C}_w$ at $w = w_0, g = g_0$ and hits the jump curve at $t = t_{g_0}$, then the trailing cell starting at $w = w_{rk}, g = g_0$ will reach $w = w_0$ at this time. The dotted horizontal lines show that at any moment the two cells lie on the same g-level.

the jump curve, and the trailing cell reaches the initial $w^\star$ value of the leading cell. It is easy to establish that $\mathcal{C}_w$ is negatively sloped in the w–g plane.

What we next want to know is whether the time interval $t_{g_0}(w^\star)$ ensuring periodicity in w agrees with the periodicity condition for the synaptic variable g_0. Note that the value of g is "slaved" to the value of D, since g is reset at a spike time to $g(t^+) = \bar{g}D(t^-) = \bar{g}D_{\max}$. Therefore periodicity in g is ensured if $D(t)$ is periodic. Thus $g_0(t_{in}^+) = \bar{g}D_{\max}$, where $D_{\max}$ satisfies the periodicity condition (11), and we obtain

$$g_0(t_{in}^+) = \frac{\bar{g}(1 - e^{-t_{in}/\tau_D})}{1 - re^{-t_{in}/\tau_D}}. \tag{13}$$

This relation can be inverted to find t_{in} as a function of g_0 given by

$$t_{in}(g_0) = \tau_D \ln \frac{\bar{g} - rg_0}{\bar{g} - g_0}. \tag{14}$$

Thus given an initial g_0 value, Eq. (14) determines the length of the interspike interval needed for the synaptic conductance to return to its original value g_0, which occurs when the spike-triggered reduction of synaptic conductance due to depression matches the recovery from depression over this interval.

To briefly summarize, for any initial value g_0 of synaptic conductance at the spike time, we have now determined two distinct inter-spike intervals associated with two different periodicity conditions: interval $t_{g_0}(w^\star)$ ensures periodicity in w, given that one of the cells is at $\mathcal{C}_w$, while the other is at w_{rk}, whereas $t_{in}(g_0)$ represents the inter-spike interval necessary for periodicity in synaptic conductance. We want to know if there exists a g_0 value (say g^*) that satisfies both periodicity conditions simultaneously, $t_{g^*}(w^\star(g^*)) = t_{in}(g^*)$. If one cell begins at (w^*, g^*) and the other at (w_{rk}, g^*), then in the time $t_{g^*}(w^\star) = t_{in}(g^*)$, the leading cell will reach the jump curve and be reset to (w_{rk}, g^*), while in the same time, the trailing cell will evolve toward the jump curve and be reset to $(w^\star, g^*)$. Thus we will have established the existence of the 2-cluster solution.

Since we already have an analytic expression for t_{in}, let us focus now on obtaining one for $t_{g_0}(w^\star)$. As noted earlier, the jump curve is negatively sloped. As in [11], we assume the jump curve is linear, and can be written as $g + Mw = c$ where M and c are the negative slope and intercept in the w–g plane. These constants can be calculated since the jump curve passes through the points $(0, \hat{g})$ and $(w_{lk}, 0)$: $M = \hat{g}/w_{lk}$, $c = \hat{g}$. Assuming that a cell starts on $\mathcal{C}_w$ at (w_0, g_0), we find that t_{g_0} satisfies

$$g_0 e^{-t_{g_0}/\tau_s} + \frac{\hat{g}w_0}{w_{lk}} e^{-t_{g_0}/\tau_w} = \hat{g}. \tag{15}$$

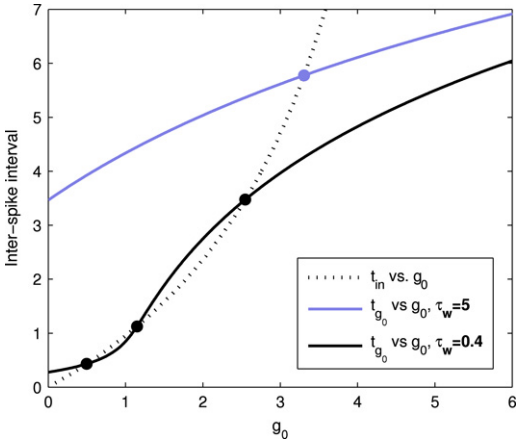

Fig. 6. The curves t_{in} and t_{g_0} for two different values of time constant τ_w. The concave up grey curve is t_{in}, the concave down curve is t_{g_0} for the case $\tau_w = 5$ and the sigmoidal curve is t_{g_0} for the case $\tau_w = 0.4$. Points of intersection of either of the t_{g_0} curves with the t_{in} curve represent 2-cluster solutions. Note that in the case of small τ_w there are multiple intersections.

In the above equation, there are three unknowns, t_{g_0}, w_0 and g_0. But the first two are related in that Eq. (12) must be satisfied. Substituting into (15), we obtain

$$g_0 e^{-t_{g_0}/\tau_s} + \frac{\hat{g}w_{rk}}{w_{lk}} e^{-2t_{g_0}/\tau_w} = \hat{g}. \tag{16}$$

Note that in (16), we now have a relationship for t_{g_0} solely as a function of the unknown g_0. This forms one of the two necessary conditions for the 2-cluster solution. The other is contained in Eq. (14). Fig. 6 shows a plot of t_{g_0} and t_{in} versus the initial conductance g_0 for two different values of τ_w. The intersection of the t_{in} curve with a t_{g_0} curve represents a 2-cluster solution where the value $t_{g_0} = t_{in}$ provides the interspike interval of the I cell or correspondingly, the time distance between the different P cells. Interestingly, in the case τ_w small, there can be three intersection points as shown in Fig. 6, yielding three potential interspike intervals for a 2-cluster solution. The existence of these three solutions was similarly found for the equivalent of a 1-cluster solution (synchronous solution) in [3]. There a single P cell was coupled to I and the three resulting solutions all had different interspike intervals as a function of the level of depression. Note that the curve t_{in} is affected only by parameters associated with the synapses from I and thus there is a single curve for both values of τ_w. The curve t_{g_0} on the other hand is affected by the synapse from I (first term on the left-hand side of (16)), the intrinsic properties of each P cell (second term on the left-hand side) and the interplay of the two ($\hat{g}$ on the right-hand side).

To get a better understanding of this, let's consider the case $g_0 = 0$, then (16) simplifies and an explicit solution for t_{g_0} can be obtained as

$$t_{g_0} = \frac{\tau_w}{2} \ln \frac{w_{rk}}{w_{lk}}. \tag{17}$$

Thus, in this case t_{g_0} is solely dependent on the intrinsic properties of each P cell, and the synapse plays no role. In general, if τ_w is very small, then t_{g_0} can be made small whenever $g_0 < \hat{g}$, not just for $g_0 = 0$, since in this case the second term on the left hand side of (16) will still dominate the determination of t_{g_0}. Thus, for small τ_w, (17) applies and one expects the curve to have near zero slope and a small value for all $g_0 < \hat{g}$. Alternatively, if τ_w is larger, then the curve t_{g_0} can be made to intersect the vertical axis $g_0 = 0$ at as large a value as one wants, consistent with what is shown in Fig. 6. Now let us consider the case $g_0 \geq \hat{g}$. If τ_w is small, the synapse is

the sole determinant of t_{g_0} in this case, and one can easily estimate t_{g_0} from (16) as

$$t_{g_0} = \tau_s \ln \frac{g_0}{\hat{g}}. \tag{18}$$

Here the value of τ_s becomes important. Small (large) τ_s implies a small (large) t_{g_0}. However, for any value of τ_s, t_{g_0} is bounded from above as g_0 is bounded by $\bar{g}$. If τ_w is not small relative to τ_s, then (16), in general, cannot be simplified. Nonetheless, it is easy to see that t_{g_0} is bounded as $g_0 \to \bar{g}$ since the first term in (16) is bounded in this limit.

Next let us consider the curve $t_{in}(g_0)$. As can be seen from (14), this curve is affected only by parameters associated with the synapse, depression and the synapse's recovery from depression. Consider two different limits, $g_0 \to 0$ and $g_0 \to \bar{g}$. In the former, $t_{in} \to 0$, while in the latter, $t_{in} \to \infty$. Moreover its easy to show that $\mathrm{d}t_{in}/\mathrm{d}g_0 > 0$. Thus the curve $t_{in}(g_0)$ is unbounded and monotone increasing. Since $t_{in}(0) = 0$, $t_{g_0}(0) > 0$, $t_{g_0}(\bar{g})$ is bounded, $t_{in}(g_0)$ is unbounded as $g_0 \to \bar{g}$ and both curves are continuous, the curves must intersect at least once. This intersection corresponds to a 2-cluster solution.

We have derived a consistency condition that must be satisfied for the 2-cluster solution. The above procedure, however, does not define a map whose fixed points correspond to a solution. Indeed, the curve t_{g_0} only yields information when the leading cell starts on $\mathcal{C}_w$ and the trailing cell starts at w_{rk}. Thus the stability of the solution cannot be obtained simply by checking the derivatives of t_{g_0} and t_{in} at a point of intersection. In Section 3.2, we will derive a two-dimensional map to assess stability of solutions.

Prior to assessing stability, let us show how the above argument can be extended to prove the existence of clusters of size $n \leq m$ in a network of m pyramidal cells. The curve t_{in} is not affected by the number of cells, nor the number of clusters in the network. The curve t_{g_0} however will be. Suppose we seek an n-cluster solution. Now instead of having a single curve $\mathcal{C}_w$, we can find $n-1$ curves $\mathcal{C}_{w_i}$. Each curve is defined so that if a cell starts on $\mathcal{C}_{w_1}$ at $t = 0$ and reaches the jump curve at $t_{g_0}(w_0)$, then a cell starting on $\mathcal{C}_{w_j}$ would reach the initial w position of the immediately preceding cell starting on $\mathcal{C}_{w_{j-1}}$ at time $t_{g_0}(w_0)$. This allows us to generalize Eq. (12) for $1 \leq j \leq n$ to

$$w_{j-1} = w_j \mathrm{e}^{-t_{g_0}/\tau_w}, \tag{19}$$

where $w_n = w_{rk}$. By successive substitutions into (19), we obtain

$$w_0 = w_{rk} \mathrm{e}^{-(n-1)t_{g_0}/\tau_w}. \tag{20}$$

Thus the time t_{g_0} for the n-cluster case must satisfy the generalization of (16) given by

$$g_0 \mathrm{e}^{-t_{g_0}/\tau_s} + \frac{\hat{g} w_{rk}}{w_{lk}} \mathrm{e}^{-n t_{g_0}/\tau_w} = \hat{g}. \tag{21}$$

Eq. (21) is valid for any $n \leq m$. For any value n, the curve of solutions satisfying (21) is qualitatively similar to the curve obtained for the 2-cluster case; see Fig. 7. The main difference is that if $n_1 < n_2$, the curve for the n_1 case lies strictly above that for the n_2 case. All of these curves will still have at least one intersection with the curve $t_{in}(g_0)$, thus guaranteeing the existence of an n-cluster solution for any $n \leq m$. Note that this argument does not depend on, nor does it determine, the size of each cluster, since the I-cell spikes only once regardless of the number of coincident inputs it receives from the synchronized P cells. For example if $m = 4$, then as discussed earlier, there can exist two distinct 2-cluster solutions displaying the same interspike interval. One has clusters of size 1 and 3 and the other has clusters of size 2 and 2.

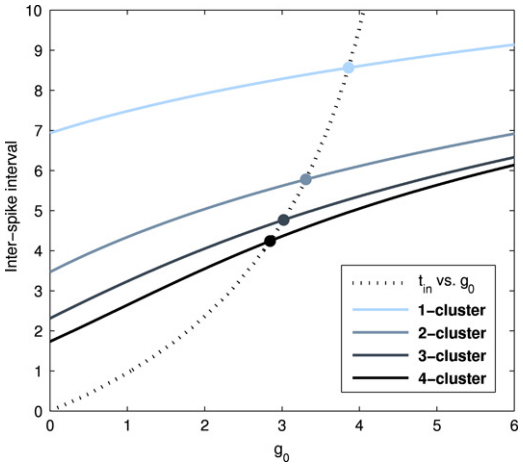

Fig. 7. Existence of multiple cluster solutions. The concave up t_{in} curve intersects the various t_{g_0} curves corresponding to solutions with different number of synchronized clusters; Eq. (21) solved for $n = 1, 2, 3$ and 4. As the number of clusters decreases, the inter-spike interval associated with the solution increases.

3.2. Stability of solutions and basins of attraction

We have shown the existence of multiple cluster solutions all for the same set of parameter values. The major question to now answer is whether any of these solutions are stable. If so, what are their basins of attraction?

Let us consider the stability of the 2-cluster solutions shown in Fig. 6. We shall do so by considering two separate cases. First, we consider the case of $m = 2$ (one cell per cluster), whereby without loss of generality we can restrict our analysis to $\Delta t = 0$. Next, we will consider a more general case of $m > 2$ and show how to reduce it to the $m = 2$ case. If $m > n$, we cannot restrict ourselves to the case $\Delta t = 0$, since all solutions will be unstable except the m-cluster solution. The reason for this is straightforward. Suppose two cells are very close to one another at the moment that one of them is at the jump curve. With zero synaptic delay, an arbitrarily small difference between these cells will be expanded since the trailing cell will be reset vertically in the w–g phase plane, while the leading cell will be reset to w_{rk}. In fact as the number of cells $m \to \infty$, an asynchronous or splay state solution ensues. Thus a non-zero synaptic delay is a necessary condition for stability of an n-cluster solution for $n < m$. This is consistent with several other modeling studies [11,21,25]. Further, in the case $n < m$ we have to consider perturbations of two different types, as explained below.

3.2.1. Stability with one cell per cluster ($m = n$), and $\Delta t = 0$

For the case $m = n = 2$, $\Delta t = 0$, consider a two cell network and define a two-dimensional map in the following way. Let the leading cell begin at an initial position $(w_1, \bar{g}D)$ and the trailing cell at $(w_{rk}, \bar{g}D)$ on the w–g slow manifold. We let the system evolve until the leading cell hits the jump curve at $t = t_{g_0}$, at which time we reset that cell to w_{rk} and both cells vertically to $g(t_{g_0}^+) = \bar{g}D(t_{g_0}^-)$ to account for the synaptic input. The vertical reset on the slow manifold is written in terms of g, but it is the periodicity of the D variable that is of interest. Thus at the moment that g is reset, we define the two-dimensional map $\Pi : (w, D) \to (w, D)$ by

$$\Pi(w, D) = [w_{rk} \mathrm{e}^{-t_{g_0}/\tau_w}, 1 - (1 - rD)\mathrm{e}^{-t_{g_0}/\tau_D}]. \tag{22}$$

A fixed point (w^*, D^*) of this map corresponds to a 2-cluster solution found through satisfaction of the periodicity conditions (14) and (21). The stability of the solution can be obtained by linearizing (22) around this fixed point and computing the

eigenvalues of the ensuing Jacobian. Denoting the Jacobian by J and evaluating it at a fixed point (w^*, D^*), we obtain

$$J = \begin{bmatrix} \dfrac{-w^*}{\tau_w}\dfrac{\partial t_{g_0}}{\partial w} & \dfrac{-w^*}{\tau_w}\dfrac{\partial t_{g_0}}{\partial D} \\ \dfrac{1-D^*}{\tau_D}\dfrac{\partial t_{g_0}}{\partial w} & r\mathrm{e}^{-t_{g_0}/\tau_D} + \dfrac{1-D^*}{\tau_D}\dfrac{\partial t_{g_0}}{\partial D} \end{bmatrix}, \tag{23}$$

where

$$\begin{aligned} \frac{\partial t_{g_0}}{\partial w} &= \frac{\frac{\hat{g}}{w_{lk}}\mathrm{e}^{-t_{g_0}/\tau_w}}{\frac{\hat{g}w^*}{w_{lk}\tau_w}\mathrm{e}^{-t_{g_0}/\tau_w} + \frac{\bar{g}D^*}{\tau_s}\mathrm{e}^{-t_{g_0}/\tau_s}} \\ &= \frac{\tau_w}{w^*}\left[1 + \frac{g^*_{\min}}{\hat{g}}\frac{\tau_w}{\tau_s}\frac{w_{lk}w_{rk}}{(w^*)^2}\right]^{-1}, \\ \frac{\partial t_{g_0}}{\partial D} &= \frac{\bar{g}\mathrm{e}^{-t_{g_0}/\tau_s}}{\frac{\hat{g}w^*}{w_{lk}\tau_w}\mathrm{e}^{-t_{g_0}/\tau_w} + \frac{\bar{g}D^*}{\tau_s}\mathrm{e}^{-t_{g_0}/\tau_s}} \\ &= \frac{\tau_s}{D^*}\left[1 + \frac{\hat{g}}{g^*_{\min}}\frac{\tau_s}{\tau_w}\frac{(w^*)^2}{w_{lk}w_{rk}}\right]^{-1} \end{aligned}$$

where $g^*_{\min} = D^*\bar{g}\exp(-t_{g_0}/\tau_s)$ is the minimal value of synaptic conductance achieved right before the spike of the I cell in each period. Stability will follow if the eigenvalues of J lie inside the unit circle in the complex plane. We note that the magnitude of the upper left entry of J is always less than one independent of parameters and the values of w^* and D^*. In general, the eigenvalues of (23) can be calculated numerically, while in certain cases they can be estimated analytically. For example, consider the case when τ_w is small and there are three 2-cluster solutions (see Fig. 6, $\tau_w = 0.4$). For the solution with the smallest interspike interval, in the limit $\tau_w \to 0$ we have $\partial t_{g_0}/\partial w \to \tau_w/w^*$, and $\partial t_{g_0}/\partial D \to \tau_w\bar{g}/\hat{g}$ (see Eq. (17) and note that $(w^*)^2/(w_{lk}w_{rk}) \to 1$). Thus, in this case J reduces to an upper triangular matrix whose eigenvalues lie on the diagonal. The upper left entry yields an eigenvalue that approaches -1 from above (factor w^*/τ_w cancels out) and therefore stays inside the unit circle for any non-zero value of τ_w. The lower right entry becomes $r\exp(-t_{g_0}/\tau_D) \to r < 1$, yielding another stable eigenvalue. Thus, this solution will be stable. We numerically calculated the eigenvalues of J for this solution in Fig. 6, and found them to be -0.67 and 0.74. For the solutions with the intermediate and the largest interspike intervals, $w^* = w_{rk}\exp(-t_{g_0}/\tau_w)$ is exponentially small in the limit $\tau_w \to 0$, since t_{g_0} remains finite (see Eq. (18)), and therefore $\partial t_{g_0}/\partial w$ would be exponentially small as well, whereas $\partial t_{g_0}/\partial D \to \tau_s/D^*$. Therefore, all elements of the Jacobian matrix will be exponentially small, apart from the lower-right element yielding the non-zero eigenvalue $r\exp(-t_{g_0}/\tau_D) + (1 - D^*)\tau_s/(D^*\tau_D)$. Note that the second term in this eigenvalue expression is a decreasing function of D^*, which in turn is an increasing function of t_{g_0}, and therefore both terms are small for the solution with the largest inter-spike interval. Numerical evaluation of the eigenvalues yields the values -5×10^{-7} and .71 for the largest interspike interval solution, versus -0.038 and 1.38 for the solution corresponding to the intermediate inter-spike interval. That one of the eigenvalues is larger than one indicates that the latter solution is unstable.

The larger $\tau_w = 5.0$ case shown in Fig. 6 is very similar to the large interspike interval case discussed above. In both cases the partial derivative $\partial t_{g_0}/\partial w$ is small and thus the solution is stable if τ_D is big enough.

3.2.2. Stability for $n < m$

We now consider the stability of a 2-cluster solution in a $m > 2$ cell network. As discussed above, in this case it is crucial to include non-zero synaptic delay Δt in the calculation of the map (22) and the ensuing Jacobian (23). The modified map is still defined at the moment that g is reset, that is Δt after an I spike, and is given by

$$\Pi(w, D) = [w_{rk}\mathrm{e}^{-(t_{g_0}+2\Delta t)/\tau_w}, 1 - (1 - rD)\mathrm{e}^{-(t_{g_0}+\Delta t)/\tau_D}]. \tag{24}$$

The eigenvalues of the ensuing Jacobian can be calculated as before and depend continuously on Δt. Thus for small $\Delta t/\tau_D$ and $\Delta t/\tau_w$, the previous results still hold.

Note that this modified map applies to perturbations of a 2-cluster solution in the $m > 2$ cell network when all cells within a cluster are subjected to the same perturbation. By first restricting to these type of perturbations, we are effectively reducing the calculation to an $m = 2$ cell network with non-zero delay Δt. However, we also have to analyze the case when all cells within a cluster are not subjected to the same perturbation. Namely, we need to determine what happens when different subsets of cells within a cluster are perturbed differently from other subsets of the cluster. We first derive conditions under which these perturbed cells remain and eventually synchronize within the same cluster. This involves obtaining an upper bound on initial differences in w values of cells that will allow them to merge into the same cluster. The analysis in [11] begins to address the issue. To understand whether two initial conditions will merge into the same cluster, let us consider again the dynamics along the w–g slow manifold. Consider two cells with initial conditions given by (w_1, g_0), (w_2, g_0), $w_1 < w_2$ and $\Delta w_0 = w_2 - w_1$; Fig. 8. Suppose the leading cell (the one starting at (w_1, g_0)) reaches the jump curve after time $t = t_f$ with $g = g_f$. The difference in the w values of the two cells at this time is $\Delta w(t_f) = \Delta w_0\exp(-t_f/\tau_w)$. We can assume the cells always have the same g level since they would end up with the same g value after the first onset of inhibition. Thus the trailing cell will also lie on the horizontal line $g = g_f$. If the trailing cell can reach the jump curve in less than Δt, it will be able to fire prior to being inhibited, resulting in the two cells being more synchronized than when they began and the two cells eventually merging into the same cluster. Let $(w_2(t_f), g_s)$ denote the point on the jump curve where the vertical line $w = w_2(t_f)$ intersects it. Let $\tilde{t}$ satisfy $g_s = g_f\exp(-\tilde{t}/\tau_s)$. The time $\tilde{t}$ is an upper bound for how long the trailing cell needs to reach the jump curve. It is an upper bound because this time is computed by assuming that the trailing cell travels vertically on the slow manifold and that its w variable does not change. Since the trajectory is not vertical, the trailing cell will actually reach the jump curve with $g > g_s$, and the time of evolution from g_f to that point will be less than $\tilde{t}$. Let $\Delta g = g_s - g_f$. Then using the linear approximation for the jump curve, $\Delta g = -M\Delta w$, we obtain

$$g_f(\mathrm{e}^{-\tilde{t}/\tau_s} - 1) = -M\Delta w_0\mathrm{e}^{-t_f/\tau_w}. \tag{25}$$

Solving for $\tilde{t}$, we obtain

$$\tilde{t} = \tau_s\ln\frac{g_f}{g_f - M\Delta w_0\mathrm{e}^{-t_f/\tau_w}}. \tag{26}$$

Thus if $\tilde{t} < \Delta t$, the trailing cell will reach the jump curve before the inhibition from the leading cell affects it. Therefore

$$\tau_s\ln\frac{g_f}{g_f - M\Delta w_0\mathrm{e}^{-t_f/\tau_w}} < \Delta t, \tag{27}$$

or alternatively

$$\Delta w_0 < \frac{g_f\mathrm{e}^{t_f/\tau_w}}{M}(1 - \mathrm{e}^{-\Delta t/\tau_s}) \tag{28}$$

provides a condition which when satisfied allows the two P cells to be in the same cluster. Thus we have shown that when cells in a cluster are arbitrarily perturbed that if they start within a neighborhood of the leading cell, they will remain in the same cluster and eventually synchronize. Thus we have reduced the

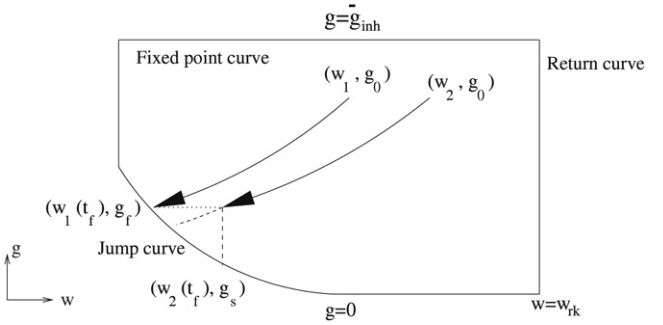

Fig. 8. Clustering of trajectories with two distinct initial conditions. At $t = 0$ the two cells start at (w_i, g_0). When the first cell reaches the jump curve at $t = t_f$, we calculate an upper bound on the time needed by the second cell to reach the jump curve, given by the time required to travel vertically to the jump curve. If this time is less than the synaptic delay time, then the two cells will merge together into the same cluster.

issue of arbitrary perturbations of the 2-cluster solution in a $m > 2$ cell network to one of assessing stability of the 2-cluster solution in a $m = 2$ cell network.

The previous argument can also be used to infer several things about the basin of attraction of a n-cluster solution in a m-cell network. First note that if $\Delta t = 0$ then (28) can never be satisfied. This implies that a synaptic delay is a necessary condition to obtain clusters of size $n < m$. Moreover as the delay $\Delta t \to 0$, (28) becomes harder to satisfy, and as a result, the basin of attraction of a n-cluster solution shrinks. Thus the m-cluster solution becomes globally attracting. Second, observe that the right-hand side of (28) grows exponentially with t_f and linearly with g_f, both of which can be estimated for a particular n-cluster solution. For example, suppose τ_s is very large, implying that the synaptic decay rate is very slow. In (28), the term $1 - \exp(-\Delta t/\tau_s)$ would be small but bounded away from zero. For this case, the synchronous, 1- and 2- cluster solutions will be the ones with the largest basin of attractions, while the solutions with more clusters will have very small basins. For the large cluster solutions, the synapse from I would be very weak and thus g_f would be small. Moreover, t_f would be determined solely by τ_w and could be small if τ_w is. Thus Δw_0 satisfying (28) would be small. Alternatively, for the synchronous or small cluster solutions, t_f would be much larger due to the fact that τ_s is now setting this time. The value g_f would also be larger since the I synapses would have more time to recover between spikes. As a result, Δw_0 would be larger than in the large cluster solution case. Therefore cells with larger differences in w can be brought together into the same cluster due to the slow decay of inhibition. In the opposite scenario where τ_s is too small, the term $1 - \exp(-\Delta t/\tau_s)$ would not be so small. Thus even when t_f and g_f are small, the right hand side of (28) isn't necessarily. Thus the large cluster solutions have larger basins of attraction in this limit.

Eq. (28) can also be used to estimate the basin of attractions of the different types of 2-cluster solutions that exist for τ_w small. In this case, based on the argument above, the 2-cluster solution with the largest interspike interval will have the largest basin of attraction. The same analysis shows that for the case τ_w small, there can exist 2 or 3 n-cluster solutions as well. Again, the one with the largest interspike interval will have the largest basin of attraction relative to the other.

3.3. A discrete map for interspike intervals

We could follow the procedure described above to derive a n-dimensional map for the n-cluster ($n \geq 3$) solutions. However, determining the stability of solutions would be computationally difficult as the Jacobian would yield an $n \times n$ matrix whose eigenvalues we would need to compute. Instead of determining stability using this potentially messy n-dimensional map, let us turn to a conceptually simpler one-dimensional approach that involves the interspike interval. Suppose we consider a network of m cells, where each cell lies on the slow manifold of the system at some initial conditions $(w_i(0), g(0))$. As time evolves, we record the time interval T at which the P cell closest to the jump curve reaches the threshold. All cells that reach the jump curve within the Δt synaptic delay interval of T are assumed to spike, and their w_i values are reset, as is the $I \to P$ synaptic conductance variable, g. This iterative process is then repeated, leading to a sequence of inter-spike intervals $\{T_j\}$. If this sequence converges to say T^*, then we will have obtained a stable solution in which the time T^* denotes the time between I spikes.

We numerically calculated such an inter-spike interval sequence by evolving four cells on the slow manifold with the linear Eq. (9), solving the equation

$$g_0 e^{-T/\tau_s} + \frac{g w_0}{w_{lk}} e^{-T/\tau_w} = \hat{g}, \tag{29}$$

for the time T needed for each cell to reach threshold. The minimal among these T values represents the next inter-spike interval, T_j. We continue to evolve the slow manifold equations during the synaptic delay interval Δt, resetting the w value of each cell that reaches the jump curve to w_{rk}. As described above, the common synaptic conductance value g is reset to $g_j = \bar{g} D(t^-)$ at time $t = T_j + \Delta t$, where $D(t)$ is evolved according to (7). One instance of this iterative process is shown in Fig. 9 in the case of $\tau_w = 0.4$ where there is bistability of two different 2-cluster solutions. In panel A, the filled circles indicate different pairs (g_j, T_j) starting with different initial conditions which are shown to converge to either of the two intersections of the curves t_{in} and t_{g_0} corresponding to the two stable periodic solutions of the network dynamics. The two curves are computed from Eqs. (14) and (21) using MATLAB with $n = 2$. This figure also demonstrates the instability of the middle fixed point. Panel B shows the dynamics of the w_i values of the two-cell network as they converge to the large-period solution. It documents how the interspike interval changes from cycle to cycle eventually converging to near $T^* = 3.5$.

We also applied this interspike interval map approach to the 4-cell case corresponding to Fig. 4 by choosing parameter values for the map and the MATLAB solutions that matched those used for our XPP simulation (values given in Appendix). In Fig. 10 we show the case of convergence to a 4-cluster solution with $T^* = 22.8$. By varying initial conditions we can obtain convergence to the other cluster solutions. The values for the interspike intervals that are obtained by this method fairly well approximate what we obtained by numerically solving the full set of equations in XPP. In particular, from (14) and (21), we obtain interspike intervals of 71, 35.5, 26.5 and 22.8 ms for the 1- through 4-cluster solutions, respectively. These compare with the values 70, 34, 30 and 27 obtained from XPP.

The method presented is conceptually simple, but yields less information about the properties of the n-cluster solution. In particular, even if we find a T^* implying the existence of a clustered solution, we have no way of *a priori* knowing how many clusters this solution will have. Of course, once we have obtained convergence to T^*, we can check the time traces of the w variables to determine the number of clusters within the solution.

3.4. The case without depression

We now consider the changes to the network behavior when the synapses from I do not exhibit synaptic depression. Consider the curve $t_{in}(g_0)$ which provided a periodicity condition for g_0. In the absence of depression, no such periodicity condition exists

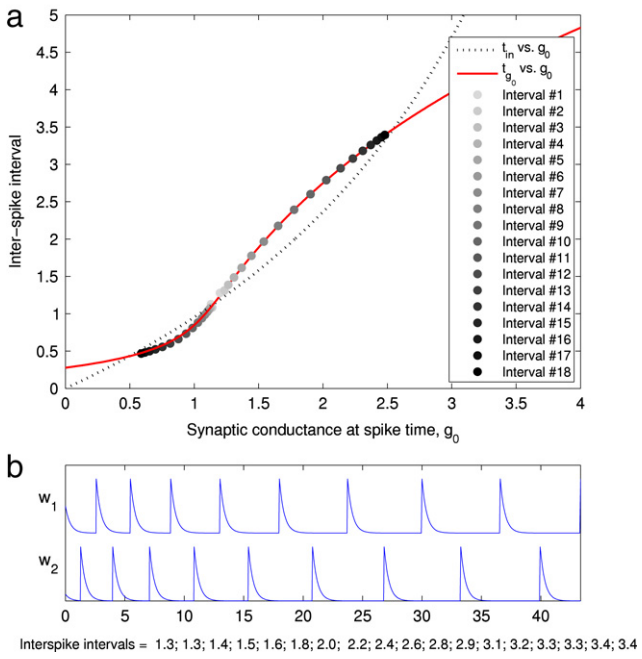

Fig. 9. Convergence to a periodic 2-cluster solution. (a) The intersections of the two curves represent the equilibrium periodic 2-cluster solutions found by solving (14) and (21). The filled circles are different iterates of the one-dimensional map of interspike intervals as they converge to either of the intersection points corresponding to stable periodic 2-cluster solutions. (b) The corresponding time traces of the recovery variable w of the two cells shows how the interspike interval approaches the value 3.5 corresponding to the large-period solution in A. Parameter values are the same as in Fig. 6 for the case $\tau_w = 0.4$.

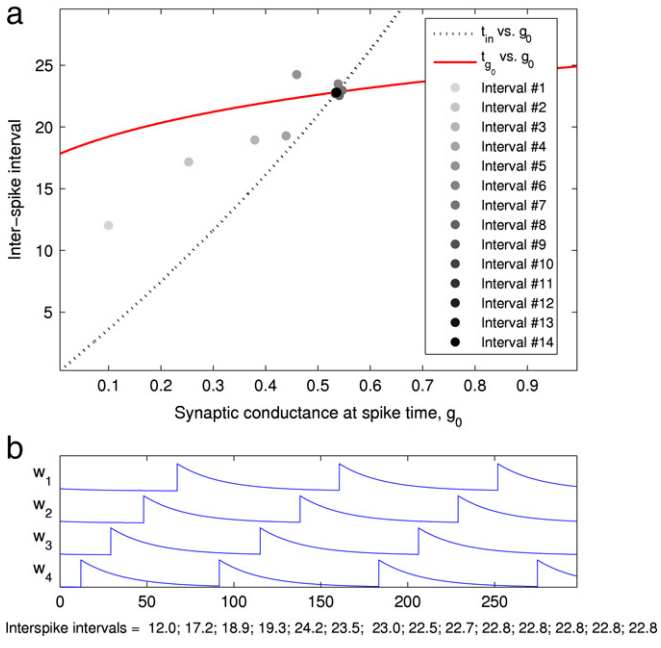

Fig. 10. Convergence to a 4-cluster solution. (a) The intersection of the two curves represents a 4-cluster periodic state found by solving (14) and (21), for parameter values approximating the conductance-based model simulation in Fig. 4b. The filled circles are different iterates of the one-dimensional map of interspike intervals as they converge to the stable intersection point. (b) The corresponding time traces of the recovery variable w of the four cells shows how the interspike interval approaches the value 22.8 corresponding to the stable periodic solution.

since whenever I fires, the synaptic conductance g is always reset to the same value $\bar{g}$. To model the case of no depression, one can either take $r = 1$ with $D \equiv 1$ or let $\tau_D \to 0$. In either limit,

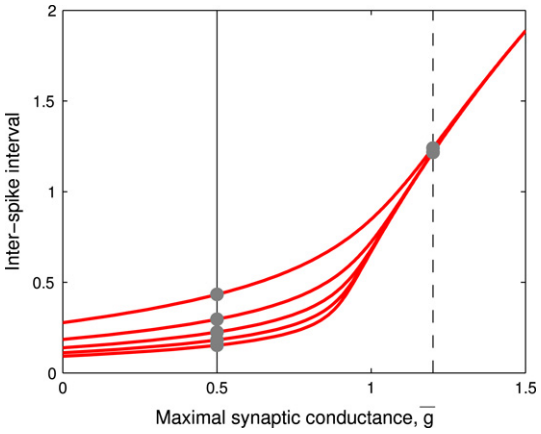

Fig. 11. Clustering in the case of non-depressing $I \to P$ synapses. Red curves show the dependence of t_{g_0} on the maximal synaptic conductance, $\bar{g}$, for solutions with $n = 2$ through $n = 6$ clusters, for the case $\tau_w = 0.4$. As the number of clusters increases, the inter-spike interval decreases. The curve corresponding to the two-cluster solution is the same as in Figs. 6 and 9. In the absence of depression, the magnitude of synaptic conductance at the spike-time is fixed, and is equal to the maximal synaptic conductance parameter (abscissa, $\bar{g}$). Vertical lines correspond to fixed values of this parameter, $\bar{g} = 0.5$ (solid line) and $\bar{g} = 1.2$ (dashed line). Note that for $\bar{g} = 1.2$, the inter-spike interval is independent of the number of clusters in the network.

the curve $t_{in}(g_0)$ simply becomes vertical at the value $g = \bar{g}$, as shown in Fig. 11. As can be seen, there still exist n-clusters solutions for all $n \leq m$, indicating that depression is not necessary for multistability. However, there are two crucial differences between the two cases. First, in the absence of depression, the distribution of interspike intervals can be very narrow. In Fig. 11, note that as $g_0 \to \infty$, the curves t_{g_0} converge to the interspike interval value $\tau_s \ln \frac{\bar{g}}{\bar{g}}$. This is because for large g_0, all cells start with $g = \bar{g}$ and must wait for the synaptic conductance to decay to at least $\hat{g}$ before a cell has access to the jump curve. Thus if $\bar{g}$ is sufficiently large (dashed vertical line), then despite the existence of distinct clustered solutions, the difference in their equilibrium interspike intervals will be small. Moreover, in this case the interspike interval will only be controlled by or be dependent on the parameters of the synapse. If $\bar{g}$ is sufficiently small (solid vertical line), then without depression the interspike intervals are more separated for clusters of different size. However these intervals are controlled by parameters associated only with P, mostly by τ_w. Thus it is harder to achieve as wide a distribution of interspike intervals as in the case with depression.

The second difference that results from the absence of depression is the loss of bistability of different n-cluster solutions. Since the curve t_{in} is now vertical, it can only intersect any particular t_{g_0} curve at one point. This loss of bistability again results from the loss of control of one set of parameters that determine the time spent in the silent state by the P cells.

Finally, note that in the absence of depression all periodic cluster states given by the intersections of the $t_{g_0}(\bar{g})$ curves with a vertical line in Fig. 11 are always stable, since the stability condition is given by the top-left element of the Jacobian in Eq. (23), which is always less than 1 in absolute value.

4. Discussion

Biological oscillatory networks often have components that interact through inhibition. This is a common feature leading to anti-phase oscillations in central pattern generating networks [15]. These types of neural circuits often involve reciprocally connected pairs of neurons. Skinner et al. [22] provided one of the earliest analytic treatments of mutual inhibition, while studying the

concepts of "escape" and "release" to describe network frequency regulation. Phase lag among inhibitory neurons within a CPG has also been widely addressed [13,23,30]. More recently, Maran and Canavier [14] and Oh and Matveev [17] have studied order-reversing rhythmic activity in networks of inhibitory neurons of type-I excitability class. Inhibitory networks can also synchronize. Wang and Rinzel [28] showed in a computational study of the thalamus that inhibitory networks could exhibit synchronous oscillations. Later Van Vreeswijk et al. [27] analytically showed how inhibition can synchronize a pair of inhibitory spiking neurons. Terman et al. [25] extended this result to a more general class of relaxation oscillators. Mutual inhibition has also been studied in concert with electrical synapses between cells [12,20]. These studies have teased out the various contributions of the chemical and electrical synapses to network behavior.

In many other neural systems, inhibition from a single neuron or groups of neurons can reach a large number of targets. For example, a variety of interneurons in the hippocampus provide feedback inhibition to a large number of pyramidal cells from whom they receive excitation [8]. In Drosophila, it is postulated that a globally inhibitory network exists to help in odor discrimination [24]. Weakly electric fish use a global feedback mechanism to discriminate between communication and prey stimuli [5]. Mathematical modeling has shed light on the role of the global inhibition in the hippocampus [11], in the thalamus [21] and in networks responsible for scene segmentation [10,29], to name only a few examples. The present study builds on these works to propose novel ways in which global inhibition can be utilized by a network.

Short-term synaptic depression is widely observed in many neuronal networks [31]. It has been shown to play a role in a variety of computational tasks, as reviewed by Grande and Spain [9]. In particular, it has been suggested to be important for sound localization and coincidence detection in the avian auditory brainstem [4], in novelty detection in the rat barrel cortex [19] and in phase maintenance in the crab pyloric network [13]. All these results provide important examples of neurons involved in temporal coding. Namely, they describe situations in which the relative timing of neuronal firing is critical for the correct functioning of that network and for downstream circuits.

Our work attempts to provide further insight on how synaptic depression can affect temporal coding properties of neural circuits. We find that depression allows a globally inhibitory network with m principal excitatory cells to maintain and transmit at least m different temporal patterns, all for the same set of parameter values. These patterns can be construed as distinct codes, with each pattern capable of being transmitted and recognized by a downstream target network. Note that in our model the patterns are distinguished both by the distinct clustering of the principal excitatory cells in each pattern, as well as by the difference in the spike frequency of the excitatory and the inhibitory cells. Depression is crucial for expanding the distribution of interspike intervals as compared to the case without it. Depression allows parameters associated with the synapses from the I cell as well as those associated with the intrinsic P cell properties to be relevant in determining interspike intervals at different frequencies. Therefore when depression is present, the downstream target can recognize each pattern based solely on the spike frequency of the inhibitory cell, or, alternatively, based on the spiking sequence of the excitatory cells. In the latter case, the coding space is much larger: given a number of clusters n smaller than the number of excitatory neurons in the network m, there are multiple distinct ways to group the m neurons into n clusters. Therefore, the total number of states is significantly greater than the number of neurons, m. This is particularly relevant if the global inhibitory network we consider is viewed as a memory circuit, with distinct activity patterns representing distinct memory states.

We derived mathematical criteria and techniques to prove the existence and stability of cluster solutions. To prove existence, we showed that when two different sets of timing constraints are met, then a cluster solution will exist. Interestingly, one of the constraints, Eq. (14), is completely controlled by the inhibitory synapses from the global inhibitor. The other constraint, Eq. (21), is determined by parameters associated with both the globally inhibitory synapse and also parameters associated with the P cells. We showed how adjusting either sets of parameters can lead to different ways in which the two constraints could simultaneously be met. Stability of the solutions was determined using a discrete map based approach. Further, the geometry of the slow manifold, namely that the jump curve is negatively sloped in the w–g phase plane, allowed us to make estimates on the basin of attraction of various solutions.

An important aspect of our modeling was a reduction to the w–g slow manifold of the system. This allowed us to solve a linear set of differential equations on that manifold to derive Eqs. (14) and (21). We then used a combination of analysis and numerics on these equations to show the existence and stability of cluster solutions. We also used the slow manifold to define low-dimensional maps. These maps are easy to numerically compute and provide information about the stability of solutions together with their basin of attraction. Despite the apparent severity of the reduction procedure, the resulting simplified model was still capable of making qualitatively and quantitatively accurate predictions for the full model. Indeed simulation results using the full set of model equations compared quite well.

Short-term synaptic plasticity and global inhibition are ubiquitous features in a variety of neural systems, in particular the mammalian cortex and hippocampus, and our results elucidate the possible functional roles of the interplay between these two properties of neural circuits. We show that such interplay can lead to highly non-trivial network activity profile, and suggest that global inhibition characterized by short-term synaptic depression can endow a neural network with a multitude of stable activity states representing different neural codes or memory states.

Acknowledgments

We thank Farzan Nadim and Jonathan Rubin for helpful discussions. This work was supported in part by the National Science Foundation grants DMS-0817703 (VM) and DMS-0615168 (AB).

Appendix

The model used to represent a single neuron (which could be excitatory or inhibitory) is based on the Hodgkin–Huxley model for the spiking neurons. This was developed by Traub and Miles [26] and then reduced to a single compartment model by Ermentrout and Kopell [7]. $C\frac{dv}{dt} = I_0 - g_l(v - V_l) - g_k w^4(v - V_k) - g_{Na} m_\infty^3(v) h(w)(v - V_{Na}) - I_{syn}$ and $\frac{dw}{dt} = [w_\infty(v) - w]/\tau_w(v)$. The gating variable for potassium activation w is defined by $w_\infty(v) = a_w(v)/[a_w(v) + b_w(v)]$ and $\tau_w(v) = \tau_w$ when the cell is in its silent phase. When the cell is in its active phase $\tau_w(v) = \tau_r$, where $\tau_w = 25$ ms and $\tau_r = 1$ ms, $a_w(v) = .032(v + 52)/\left(1 - e^{-\frac{v+52}{5}}\right)$ and $b_w(v) = .5e^{-\frac{57+v}{40}}$. The sodium activation curve at steady state is given by $m_\infty(v) = a_m(v)/[a_m(v) + b_m(v)]$ where $a_m(v) = .32(v + 54)/\left(1 - e^{-\frac{v+54}{4}}\right)$ and $b_m(v) = .28(v + 27)/\left(e^{\frac{v+27}{5}} - 1\right)$. The inactivation curve is given by $h = \max(1 - 1.25w, 0)$. The parameter values used in the simulations of Fig. 4 are: $C = 1\ \mu F\ \text{cm}^{-2}$, $g_{Na} = 100$ ms cm^{-2}, $V_{Na} = 50$ mV,

$g_K = 80$ ms cm^{-2},$V_K = -100$ mV, $g_L = .1$ ms cm^{-2}, $V_L = -65.625$ mV for the pyramidal cells and $V_L = -64.6$ mV for the interneuron. The injected current $I_0 = 0.5$ for the pyramidal cells and $I_0 = -0.5$ for the interneuron. The synaptic delay $\Delta t = 0.5$. The synaptic parameters are $\bar{g}_{inh} = 2$ ms cm^{-2}, $E_{inh} = -80$ mV, $\bar{g}_{exc} = 5$ ms cm^{-2} and $E_{exc} = 0$ mV, $\tau_D = 100$ ms and $\tau_s = 5$ ms. We use XPP [6] for the simulations associated with Fig. 4. To account for a non-zero spike width, we used a model for depression due to Bose et al. [3]. We let D evolve in the silent state of I using $D' = (1 - D)/\tau_D$, as in Eq. (7). In the active state of I, we let $D' = -D/\tau_{DI}$ where $\tau_{DI} = 1$. We use MATLAB (Mathworks, Inc.) to solve the equilibrium conditions (14) and (21). For Figs. 6 and 7, we set $r = .6$, $\tau_w = 5$, $\tau_s = 3$, $\tau_D = 10$, $\bar{g}_{inh} = 5$, $\hat{g} = .8$, $w_{lk} = .2$ and $w_{rk} = .8$. In Fig. 10 where we compare the simulations of the full model with the discrete map iteration, we take $r = .236$. This value is calculated by noting that in the simulations, each action potential has length of about 1.2 ms. We let $r = \exp(-1.2/\tau_{DI})$, where $\tau_{DI} = 1$. We also chose the values of $\hat{g} = .01$, $w_{lk} = .05$ and $w_{rk} = .85$ by estimating these values from our simulations. All numerical codes are available at the Model DB website: http://senselab.med.yale.edu/modeldb/default.asp.

References

[1] L. Abbott, J. Varela, K. Sen, S. Nelson, Synaptic depression and cortical gain control, Science 275 (1997) 220–223.
[2] W. Bialek, F. Rieke, R. de Ruyter van Steveninck, D. Warland, Reading a neural code, Science 252 (1991) 1854–1857.
[3] A. Bose, Y. Manor, F. Nadim, Bistable oscillations arising from synaptic depression, SIAM J. Appl. Math. 62 (2001) 706–727.
[4] D. Cook, P. Schwindt, L. Grande, W. Spain, Synaptic depression in the localization of sound, Nature 421 (2003) 66–70.
[5] B. Doiron, M. Chacron, L. Maler, A. Longtin, J. Bastian, Inhibitory feedback required for network oscillatory responses to communication but not prey stimuli, Nature 421 (2003) 539–543.
[6] B. Ermentrout, Simulating, Analyzing, and Animating Dynamical Systems: A Guide to XPPAUT for Researchers and Students, SIAM, Philadelphia, PA, 2002.
[7] B. Ermentrout, N. Kopell, Fine structure of neural spiking and synchronization in the presence of conduction delays, Proc. Natl. Acad. Sci. USA 95 (1998) 1259–1264.
[8] T. Freund, G. Buzsaki, Interneurons of the hippocampus, Hippocampus 6 (1996) 437–470.
[9] L. Grande, W. Spain, Synaptic depression as a timing device, Physiology 20 (2005) 201–210.
[10] D. Horn, I. Opher, Temporal segmentation in a neural dynamical system, Neur. Comp. 8 (1996) 375–391.
[11] S. Kunec, A. Bose, High-frequency, depressing inhibition facilitates synchronization in globally inhibitory networks, Network: Comput. Neural Syst. 14 (2003) 647–672.
[12] T. Lewis, J. Rinzel, Dynamics of spiking neurons connected by both inhibitory and electrical coupling, J. Comput. Neurosci. 14 (2003) 283–309.
[13] Y. Manor, A. Bose, V. Booth, F. Nadim, The contribution of synaptic depression to phase maintenance in a model rhythmic network, J. Neurophysiol. 90 (2003) 3513–3528.
[14] S. Maran, C. Canavier, Using phase resetting to predict 1:1 and 2:2 locking in two neuron networks in which firing order is not always preserved, J. Comput. Neurosci. 24 (2008) 37–55.
[15] E. Marder, R. Calabrese, Principles of rhythmic motor pattern generation, Physiol. Rev. 76 (1996) 687–717.
[16] M. Mishchenko, N. Rozov, Differential Equations with a Small Parameter and Relaxation Oscillations, Plenum, New York, 1980.
[17] M. Oh, V. Matveev, Loss of phase-locking in non-weakly coupled inhibitory networks of type-I model neurons, J. Comput. Neurosci. (2008), in press (doi:10.1007/s10827-008-0112-8).
[18] J. O'Keefe, Place units in the hippocampus of the freely moving rat, Exp. Neurol. 51 (1976) 78–109.
[19] C. Petersen, Short-term dynamics of synaptic transmission within the excitatory neuronal network of rat layer 4 barrel cortex, J. Neurophysiol. 87 (2002) 2904–2914.
[20] B. Pfeuty, G. Mato, D. Golomb, D. Hansel, The combined effects of inhibitory and electrical synapses in synchrony, Neural Comput. 17 (2007) 633–670.
[21] J. Rubin, D. Terman, Analysis of clustered firing patterns in synaptically coupled networks of oscillators, J. Math. Biol. 41 (2000) 513–545.
[22] F. Skinner, N. Kopell, E. Marder, Mechanisms for oscillation and frequency control in reciprocally inhibitory model neural networks, J. Comput. Neurosci. 1 (1994) 69–87.
[23] F. Skinner, B. Mulloney, Intersegmental coordination of limb movements during locomotion: Mathematical models predict neural circuits underlying swimmeret beating, J. Neurosci. 18 (1998) 3831–3842.
[24] A. Silbering, C. Galizia, Processing of odor mixtures in the Drosophila antennal lobe reveals both global inhibition and glomerulus-specific interactions, J. Neurosci. 27 (2007) 11966–11977.
[25] D. Terman, N. Kopell, A. Bose, Dynamics of two mutually coupled slow inhibitory neurons, Physica D 68 (1998) 241–275.
[26] R. Traub, R. Miles, Neuronal Networks of the Hippocampus, Cambridge University Press, Cambridge, 1991.
[27] C. Van Vreeswijk, L. Abbott, B. Ermentrout, When inhibition not excitation synchronizes neural firing, J. Comput. Neurosci. 1 (1994) 313–321.
[28] X. Wang, J. Rinzel, Spindle rhythmicity in the reticularis thalamic nucleus: Synchronization among mutually inhibitory neurons, Neuroscience 53 (1993) 899–904.
[29] D. Wang, D. Terman, Locally excitatory globally inhibitory oscillatory networks, IEEE Trans. Neur. Net. 6 (1995) 283–286.
[30] T. Williams, K. Sigvardt, N. Kopell, B. Ermentrout, M. Rembler, Forcing of coupled nonlinear oscillators: Studies of intersegmental coordination in the lamprey locomotor central pattern generator, J. Neurophysiol. 64 (1990) 862–871.
[31] R. Zucker, W. Regehr, Short-term synaptic plasticity, Annu. Rev. Physiol. 64 (2002) 355–405.